

# Germanium Nanowires As Anode Material for Lithium-Ion Batteries With Ability To Charge At Subzero Temperatures

Ilya Gavrilin,<sup>\*[a, b]</sup> Ivan Marinkin,<sup>[b]</sup> Alexander Skundin,<sup>[a]</sup> Tatiana Kulova,<sup>[a]</sup> Alexander Pavlikov,<sup>[c]</sup> Lidiya Volkova,<sup>[d]</sup> Roman Volkov,<sup>[b]</sup> Nickolay Borgardt,<sup>[b]</sup> Alexey Merkulov,<sup>[e]</sup> Filipp Napolksiy,<sup>[e]</sup> Anna Rudnykh,<sup>[e]</sup> and Victor Krivchenko<sup>[e]</sup>

The aim of this work is to study of germanium nanowires as low temperature and high charging rate lithium-ion battery anode material. Using a full cell with a cathode based on NMC811 and an anode based on synthesized germanium nanostructures in combination with the proposed electrolyte composition, we

demonstrate the ability to charge and cycle the battery at temperatures as low as  $-40^{\circ}\text{C}$ . The results generally indicate that using germanium nanowires as anode material in lithium-ion batteries may solve the problem of their reversible and safe charging at sub-zero temperatures.

## Introduction

Lithium-ion batteries (LIBs) are currently the most demanded secondary power sources used in a wide range of applications, from portable electronics to the automotive industry. The rapid development of LIB applications requires increasingly stringent conditions of use, such as higher energy density, fast charging and efficient operation at sub-zero temperatures.<sup>[1,2]</sup>

However, modern commercial LIBs with a graphite-based negative electrode (anode) degrade significantly during fast charging (at temperatures above zero) due to lithium plating on anode surface. This leads to both the formation of dendrites, which can cause a short circuit inside the battery, and to additional electrolyte reduction on fresh lithium surface.<sup>[3,4]</sup>

Charging a Li-ion battery with a graphite anode at low temperatures exacerbates these problems due to reduced ionic conductivity, increased desolvation energy, and slow diffusion in both the electrolyte and the solid electrode material. Slow diffusion of Li ions will lead to a significant increase in overvoltage and accelerate Li deposition on the graphite anode surface.<sup>[5,6]</sup>

Recently, most studies have focused on optimizing the electrolyte composition with new lithium salts, organic solvents and/or additives, which have extended the LIB capabilities into

the lower temperature range.<sup>[7-9]</sup> However, ion conductivity in solid electrode materials and solid electrolyte interphase (SEI) is the predominant factor for capacity degradation at low temperatures.<sup>[10,11]</sup> In addition, electrolyte optimization can increase its ion conductivity and prevent freezing, but the capacity loss caused by electrode polarization at low temperature is still unavoidable.<sup>[12]</sup>

The use of lithium titanate ( $\text{Li}_4\text{Ti}_5\text{O}_{12}$ ) as an anode material for lithium-ion batteries ensures their performance at subzero temperatures.<sup>[13,14]</sup> This anode material offers several advantages, such as stability of capacity over long cycling and high discharge currents. However, there are also some drawbacks associated with structural features of  $\text{Li}_4\text{Ti}_5\text{O}_{12}$ . For example, the high operating voltage of lithium titanate (1.55 V) and its low specific capacity significantly reduce the overall energy density of the battery. This can be a significant disadvantage in certain applications.

Therefore, in addition to the electrolyte composition, new electrode materials for low-temperature applications with high specific capacity and high ionic conductivity should be investigated.<sup>[15]</sup> Several negative electrode materials including silicon have been evaluated at low temperatures.<sup>[16-25]</sup> However, their reversible specific capacity is very low at  $-20^{\circ}\text{C}$ . At the same time, a rather low diffusion coefficient of  $\text{Li}^+$  ions in a crystal structure of such materials leads to low charge/discharge rates at low temperatures.

Due to its high specific capacity, lithium metal is a promising anode material. However, there are significant limitations to the practical use of lithium anodes due to the heterogeneous electrodeposition of lithium ions during charging and the formation of dendritic precipitates. At the same time, a decrease in the operating temperature dramatically affects the nucleation and growth of the lithium layer.<sup>[26]</sup>

Besides lithium and silicon, germanium is a very promising negative electrode material, which has a specific capacity of about 1600 mAh/g.<sup>[27-34]</sup> It is worth noting that Ge has a higher electronic conductivity<sup>[35]</sup> as well as 400 times higher lithium diffusion coefficient<sup>[36,37]</sup> compared to silicon. These features of Ge in combination with the possibility of obtaining nano-

[a] I. Gavrilin, Prof. A. Skundin, Prof. T. Kulova  
Frumkin Institute of Physical Chemistry and Electrochemistry Russian Academy of Sciences,  
31-4 Leninsky prospect, 119071 Moscow, Russia  
E-mail: gavrilin.ilya@gmail.com

[b] I. Gavrilin, I. Marinkin, R. Volkov, N. Borgardt  
National Research University of Electronic Technology (MIET),  
Bld. 1, Shokin Square, Zelenograd, Moscow, 124498, Russia

[c] A. Pavlikov  
Faculty of Physics, M.V. Lomonosov Moscow State University,  
Leninskie Gory, Moscow 119991, Russia

[d] L. Volkova  
Institute of Nanotechnology of Microelectronics of the Russian Academy of Sciences INME RAS, Moscow, 19991 Moscow, Russia

[e] A. Merkulov, F. Napolksiy, A. Rudnykh, V. Krivchenko  
Dubna State University, Dubna, Moscow Region, 141982 Russia

structured particles determine the prospects for its use in lithium-ion batteries and opens up prospects for safe fast charging, including that at sub-zero temperatures.

One of the main challenges limiting the practical use of germanium in LIBs is its volumetric expansion during the lithiation process. This expansion can be as high as 220%, which can lead to significant damage of the anode layer during cycling.

As a solution of this problem, researchers suggested application of diverse nanostructured materials including nanowires and nanoparticles, which can withstand large material expansion/contraction during alloying/de-alloying thus enabling the mechanical stability of the electrodes during hundreds of charge/discharge cycles. For a more in-depth exploration of the effects of germanium nanostructures and their synthesis methods on electrochemical properties, readers are referred to the relevant reviews.<sup>[38–41]</sup>

In addition, researchers have focused on the performance of germanium anodes at low temperatures. Germanium nanowires that are grown directly on a stainless steel current collector using a vapor-solid-solid (VSS) process have been shown to have excellent electrochemical stability in full cells with a LiCoO<sub>2</sub>-based cathode over a wide temperature range (−40 to +40 °C).<sup>[42]</sup>

Coin cells consisting of the mesoporous Ge anode prepared by a zincothermic reduction and an LiFePO<sub>4</sub> cathode have shown an excellent cyclability at −20 and 25 °C.<sup>[43]</sup>

Recently, we have shown that Ge nanowires (NWs) synthesized by simple cathodic deposition from aqueous solutions of germanium dioxide demonstrate a specific delithiation capacity at room temperature of about 1300 mAh/g at current range 1 C–4 C and about 850 mAh/g at 24 C, as well as good low-temperature performance 255 mAh/g at −50 °C in 1 M solution of LiClO<sub>4</sub> in a propylene carbonate – dimethoxyethane mixture (7:3).<sup>[44]</sup> Also, we demonstrated operation of full cell with an anode based on Ge NWs, and cathode based on LiNi<sub>0.8</sub>Co<sub>0.15</sub>Al<sub>0.05</sub>O<sub>2</sub> (NCA) at −55 °C.<sup>[45]</sup>

In this work, we study the electrochemical performance of germanium nanowires as anode material at high rates of both lithiation and delithiation. During the experiments, the current density of the lithiation/delithiation reached 32 A/g, with a specific discharge capacity of 270 mAh/g. This opens up prospects for using the germanium nanowires in lithium-ion batteries with fast charge rate.

Using coin cells with a cathode based on NMC811 and an anode based on synthesized germanium nanowires, we demonstrate the ability to charge and cycle the battery at temperatures as low as −40 °C. To demonstrate the scalability of the electrochemical system studied in this work, we fabricated a pouch cell prototype that has been cycled at temperature range −20 °C to +25 °C.

## Results and Discussion

### Electrolyte Selection

The electrolyte is one of the key components of a lithium-ion battery that determines its performance over a wide temperature range. The electrolyte components should provide the formation of stable SEI with high mechanical strength and high ionic conductivity. In this work we used LiDFOB as a salt. This salt is known to improve the structure and stability of SEI at graphite and lithium metal and CEI at oxide-based cathodes.<sup>[46–48]</sup> We hypothesise that the use of LiDFOB will also provide an efficient germanium anode operation. As additives, we used FEC, which also promotes the formation of mechanically robust SEI due to the formation of LiF on the anode surface<sup>[49–52]</sup> and VC, which promotes Coulombic efficiency at the first cycle.<sup>[52,53]</sup> A mixture of propylene carbonate (melting point −48.8 °C) and dimethoxyethane (melting point −58 °C) was used as a solvent to ensure the performance of the electrolyte at sub-zero temperature. Measurements of the ionic conductivity of the electrolyte showed that the conductivity of the electrolyte was of 0.8 mS/cm at −40 °C and increased to 8.6 mS/cm at +60 °C.

### Morphological and Physical Studies before Cycling

Figure 1a, b shows SEM images of an array of Ge nanowires obtained by electrochemical deposition from GeO<sub>2</sub> aqueous solution on a copper substrate.

As can be seen, the sample is an array of nanowires with a predominant diameter of about 40 nm. The thickness of the array is not uniform (Figure 1 b) and varies from 3 to 6 μm. In addition, areas of higher thickness up to 18 μm, can also be observed.

TEM image and the diffraction patterns obtained from nanowires are shown in Figure 1c. Analysis of the positions of the diffraction rings relative to the central electron beam revealed that the nanowires contained a polycrystalline germanium phase (insert, Figure 1c). The lattice parameter is 0.566 nm. Quantitative X-ray spectral analysis indicated the absence of indium atoms (about 8 at.%) in the nanowires.

Raman spectroscopy data also confirm the presence of a germanium crystalline phase in the sample. Only a peak in the region of 291 cm<sup>−1</sup>, which is related to germanium, is recorded on the Raman spectrum (Figure 1 d). The shift to 9 cm<sup>−1</sup> relative to bulk germanium (peak at 300 cm<sup>−1</sup>) is due to the small crystallite sizes of the material, i.e. germanium nanowires have a nanocrystalline structure with crystallite sizes of about 2 nm. That does not contradict the results obtained in our previous works.<sup>[44,54]</sup>

### Galvanostatic Cycling

Figure 2a shows the galvanostatic charge-discharge curves for the germanium anode at a current density of 0.125 A/g. It can

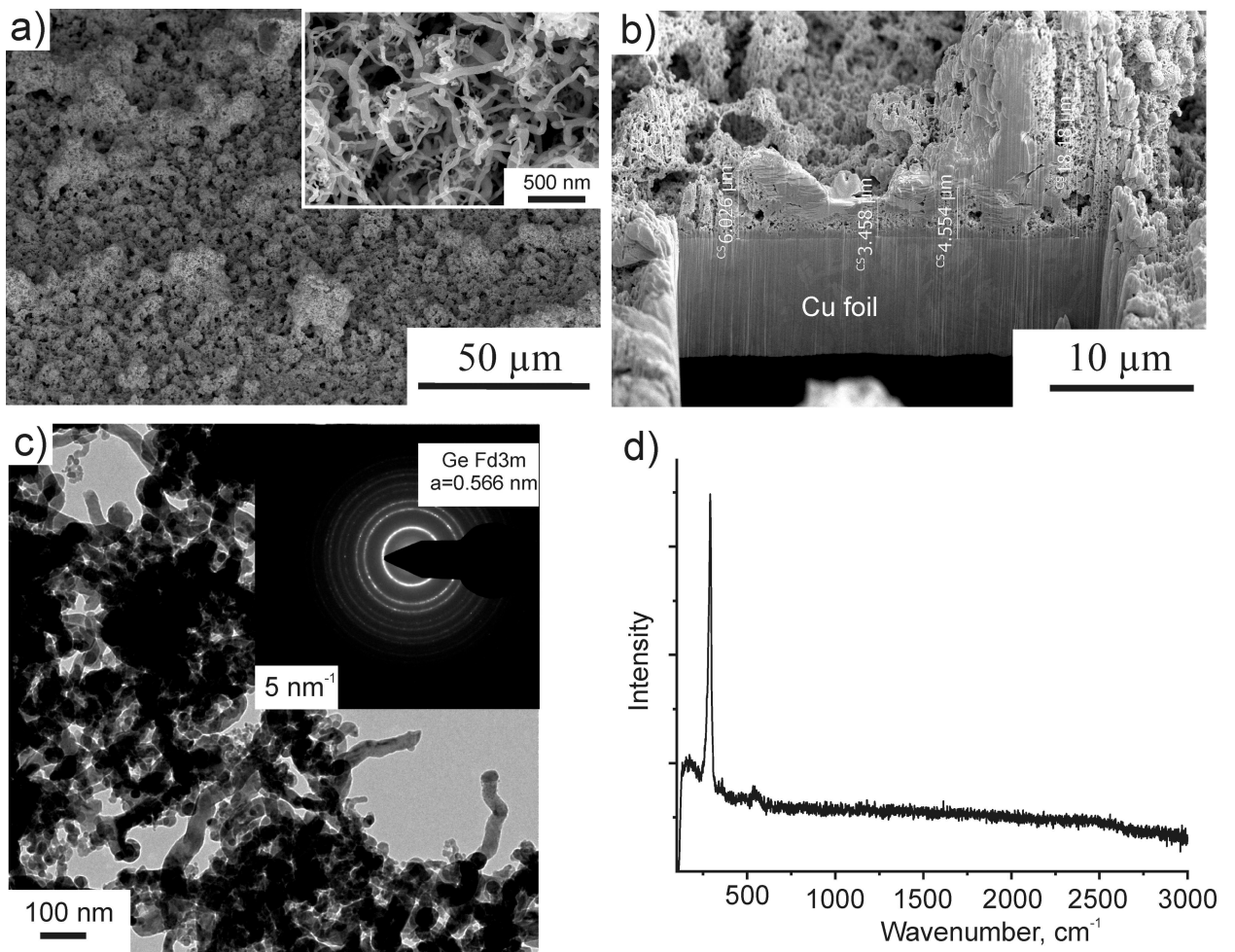


**Figure 1.** SEM images of the surface morphology (a) and cross-section (b) and TEM image (c) of a GeNWs on a copper substrate and the corresponding Raman spectrum (d). The diffraction pattern from a 1 μm diameter region is shown in the inset of Figure 1c.

be seen that the specific lithiation capacity at the first cycle reaches up to 1550 mAh/g, which is close to the theoretical value. Meanwhile, the irreversible capacity at the first cycle is 18%. The specific lithiation capacity at the second and fifth cycles was approximately of 1315 mAh/g at a current density of 0.125 A/g. The germanium anode showed excellent rate capability. During the experiments, the current density of the lithiation/delithiation reached 32 A/g, with a specific discharge capacity of 270 mAh/g. When the lithiation/delithiation current was further decreased to 0.25 A/g, the specific capacity almost returned to the same value. In addition, the stability of the material during long-term cycling was investigated with current density 1 A/g. The specific capacity does not change significantly within 100 cycles (insert, Figure 2b). This indicates that the active material has formed a very stable structure capable of withstanding volume changes without pulverisation and without loss of contact with the current collector. Further, the negative electrode based on the obtained germanium structures was tested in a half-cell (vs. lithium) at different lithiation/delithiation current. Figure 3a shows the dependences of the anode specific capacity on a number of cycles at lithiation current of 1 and 2 A/g (corresponds to the charge of a full

lithium-ion battery) and the delithiation current of 0.5 A/g (corresponds to the discharge of a full lithium-ion battery).

As can be seen from Figure 3a, during anode lithiation at 1 A/g and delithiation at 0.5 A/g, the corresponding anode specific capacities are approximately of 1308 and 1285 mAh/g, respectively. The specific capacity does not change significantly within 25 cycles. After increasing the lithiation current to 2 A/g, the anode specific lithiation capacity decreased by 17% to about 1070 mAh/g. After decreasing the lithiation current again to 1 A/g, the anode specific lithiation capacity was approximately 1203 mAh/g, which is only 8% lower than the specific capacity within the first 25 cycles. This indicates the structural stability and reversibility of the capacitive characteristics of the investigated material.

Figure 3b shows the dependence of the specific capacity of germanium anode on a number of cycles at delithiation current of 1 and 2 A/g (corresponding to the discharge of a full lithium-ion battery) and the same lithiation current of 0.5 A/g (corresponding to the discharge of a full lithium-ion battery). The lithiation and delithiation anode specific capacities were of about 1224 and 1198 mAh/g, respectively, and practically did not change within 25 cycles. When the delithiation current was

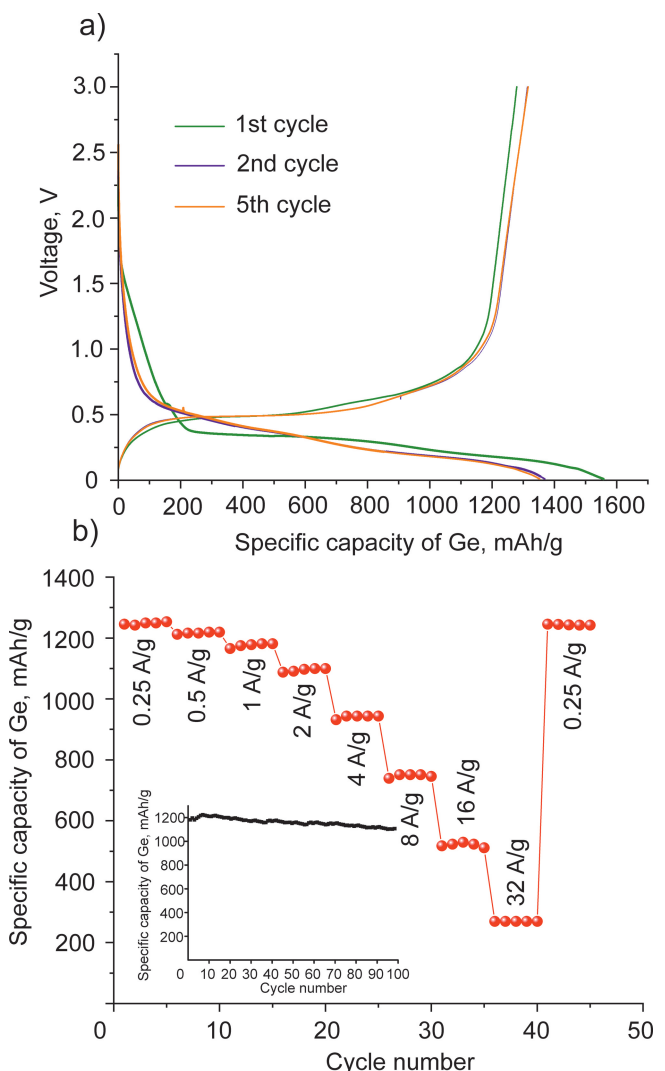


**Figure 2.** Charge-discharge curves at the 1st, 2nd and 5th cycles (a) and the rate capability at symmetric charge/discharge current (b) of a Ge nanowires/lithium half-cell. The inset of Figure 2b shows the variation of anode (discharge) capacity upon cycling with current density 1 A/g.

increased to 2 A/g, both specific capacity decreased slightly by approximately 5%. When the delithiation current was further decreased to 1 A/g, the specific capacity almost returned to the same value as during first 25 cycles. This also indicates the stability of the investigated anode material in these current regimes.

Figure 3c shows the galvanostatic charge-discharge curves for the 5th and 35th cycles. In general, the shape of the curves does not change with increase of lithiation current (Figure 3 a, c). The potential corresponded to the half-capacity as a measure of polarization is a rather informative quantity. Thus, potential decreased from 0.23 V to 0.15 V during anode lithiation, while it increased from 0.56 V to 0.61 V during anode delithiation.

Figure 3d shows the charge-discharge curves for the 5th and 35th cycles. In general, the shape of the charge-discharge curves does not change with increase in delithiation current. The average potential increased from 0.22 V to 0.28 V during

lithiation, and increased from 0.57 V to 0.64 V during delithiation.

The Coulomb efficiency in all cycling regimes was approximately of 98.5–99%. This indicates that the electrolyte composition used is effective in terms of forming a stable and mechanically robust SEI.

High anode specific capacity, which is about 1100 mAh/g, at lithiation current 2 A/g and 270 mAh/g at 32 A/g opens the prospect of using this material for lithium-ion batteries with the opportunity of faster charging rate than lithium-ion batteries with graphite anode, for which the nominal charge current is usually in the range of 0.18–0.37 A/g.

In order to study low temperature electrochemical properties of Ge NWs-based electrodes, they were tested in full coin cells with a cathode based on NMC 811 with the same electrolyte composition in the voltage range of 2.6–4.2 V at different temperatures. At the first stage, the coin cell was charged and discharged at room temperature at a current density of 0.125 A/g based on germanium mass loading on the copper current collector. The irreversible capacity at the first cycle was approximately 20%. The cell was discharged at current of 0.25, 0.5 and 1 A/g. At the next stage, the cell was charged and discharged in similar modes at –20 °C and –40 °C. The obtained results are presented in Figure 4.

Figure 4a shows the charge-discharge curves at the 1st, 2nd, 7th, 12th and 18th cycles. As can be seen, the difference between the average charge and discharge voltage (the coin cell overvoltage) practically does not depend on the discharge current and is approximately of 0.35 V. Increase in discharge current density from 0.125 to 1 A/g leads to a 22% decrease in the discharge specific capacity to about 810 mAh/g based on the mass loading of germanium. When the cycling temperature was lowered to –20 °C, the charge-discharge curve profile of the coin cell remained practically unchanged. At the same time, the discharge specific capacity of germanium anode was of 620 mAh/g at a current density of 0.25 A/g. Lowering the temperature leads to a feasible variation in the discharge specific capacity of the coin cell with increase in discharge current density (Figure 4c, d). Thus, at a current density of 1 A/g, the discharge specific capacity of germanium anode was approximately of 480 mAh/g.

It is worth noting the rather stable behaviour of the discharge characteristics of the coin cell. When the discharge current density was set again at 0.25 A/g, the specific discharge capacity almost returned to its primary value. In turn, the overvoltage on the cell increased to 0.5 V.

Decreasing the temperature to –40 °C leads to a further decrease in the coin cell capacity. The discharge specific capacity of germanium anode at current densities 0.25, 0.5 and 1 A/g were 170, 87 and 27 mAh/g, respectively. It should be noted that over the entire cycling range at –40 °C, the Coulombic efficiency was approximately of 98.5%. Lowering the temperature resulted in a further increase in the overvoltage on the cell. However, the magnitude of the overvoltage varied weakly with increasing discharge current. At a current of 0.25 A/g, the overvoltage was 1.17 V, and increased to 1.3 V when the discharge current was increased to 1 A/g.

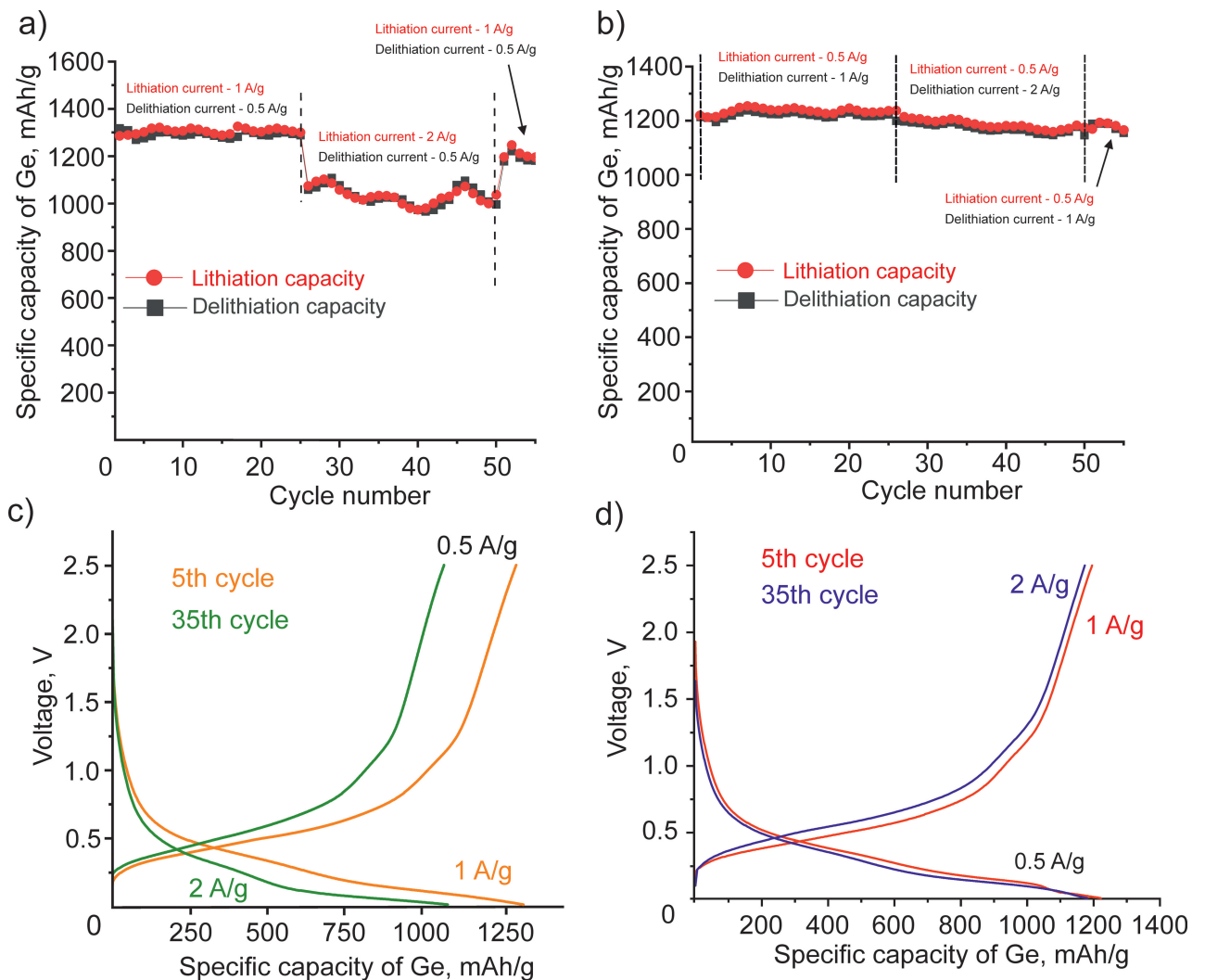


Figure 3. The rate capability (a, b) and charge-discharge curves (c, d) of the Ge NWs/lithium half-cell.

The cycling data at sub-zero temperatures indicate the stability of the electrochemical and structural characteristics of the germanium-based negative electrode. At the same time, the decrease in discharge capacity and increase in overvoltage on the cell are due to the increase in internal resistance, apparently, primarily due to a decrease in the ionic conductivity of the electrolyte.

The results of the SEM study of anode morphology after cycling at different temperatures and different charge/discharge rates in a coin cell with a cathode based on NMC811 showed that the structure of the sample is a fairly dense layer with a thickness of about 10  $\mu\text{m}$  (Figure 5a). The germanium nanowires in the images shown are apparently not visible because they are located in a layer of electrochemical reaction products that could not be washed away. It should be noted that under the action of the electron beam, this layer has apparently decomposed and evaporated. At the same time, Raman spectroscopy shows that the crystallinity of germanium is preserved. A peak in the  $289 \text{ cm}^{-1}$  region, which is attributed to germanium crystal lattice, is clearly seen on the Raman

spectrum (Figure 5b). The  $11 \text{ cm}^{-1}$  shift relative to bulk germanium (peak at  $300 \text{ cm}^{-1}$ ) corresponds to a crystallite size of about 1 nm.

As illustrated in Figure 5c, the HAADF image and elemental distribution maps of the sample reveal the absence of maps depicting the distribution of carbon forming epoxy resin (1, Figure 5c). Furthermore, the observation of germanium nanowires in their original shape and size was not possible. However, filamentous nanoobjects (with diameters ranging from a few units to tens of nanometres) with a dendritic structure were identified (2, Figure 5c).

A comparison of the elemental distribution maps reveals that the filamentary nanoobjects are composed of germanium, with an elevated concentration of oxygen, seemingly a constituent of germanium oxide, observed on their surface. Quantitative XRD analysis demonstrated that the germanium oxide located on the surface of the filamentous nanoobjects is stoichiometric and has the chemical formula  $\text{GeO}_2$ . The presence of  $\text{GeO}_2$  is characteristic of all the samples and is most likely associated with the oxidation of the samples upon the

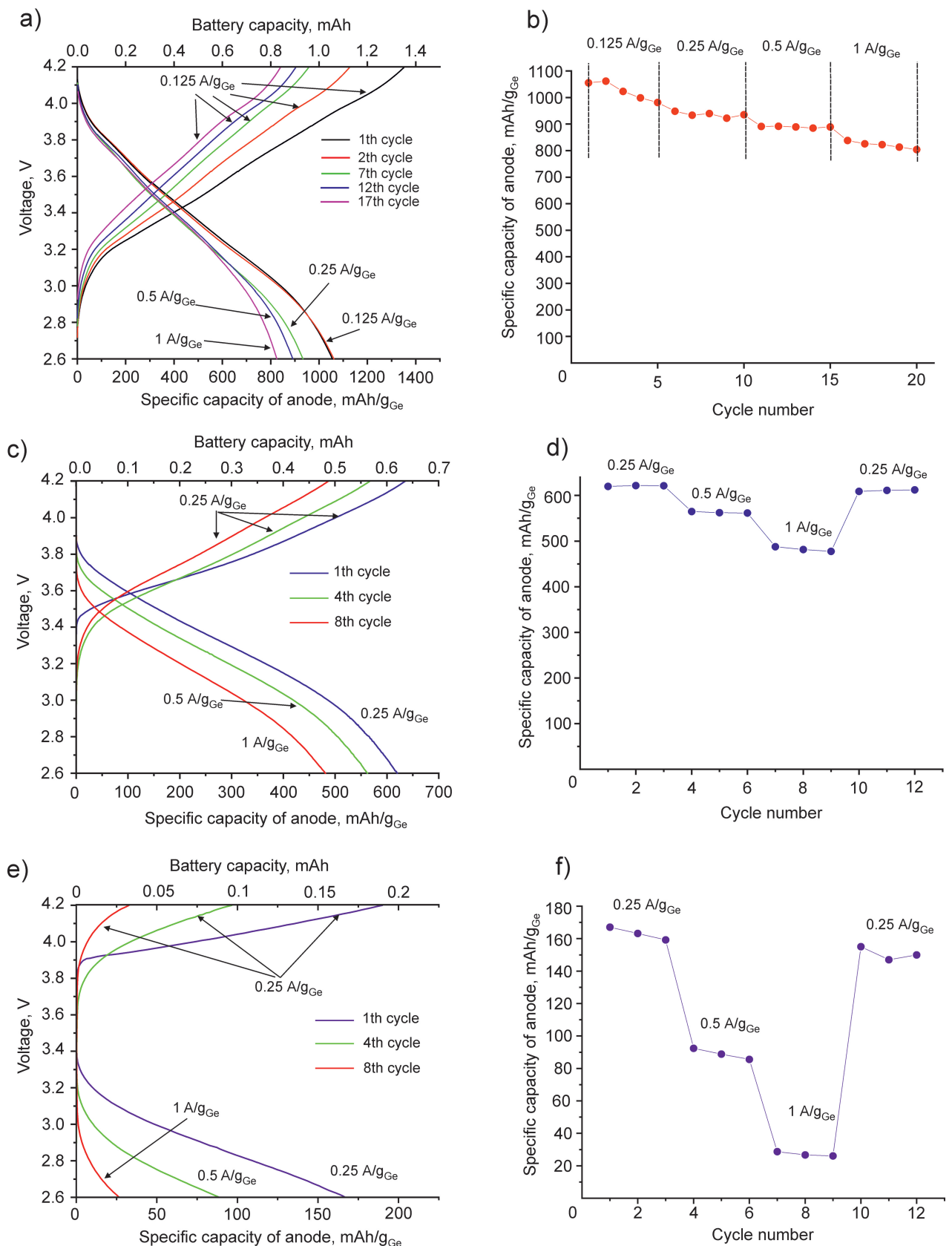


**Figure 4.** Galvanostatic charge-discharge curves and rate capability of the Ge NWs anode in the NMC 811/Ge NWs full coin cell at different temperatures: 20 °C (a, b); -20 °C (c, d) and -40 °C (e, f).

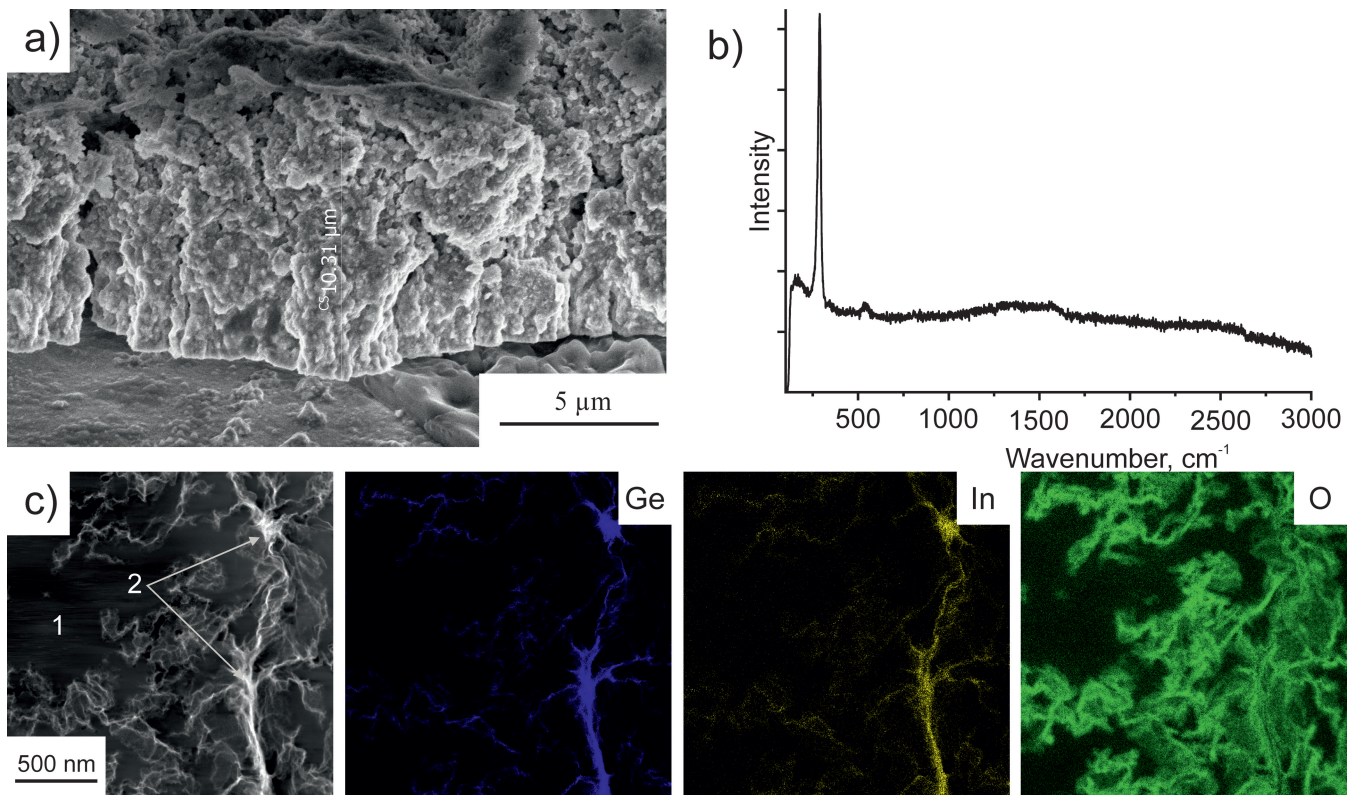


**Figure 5.** SEM image of the cross-section (a) and the corresponding Raman spectrum (b) of the sample after cycling at different temperatures and different charge/discharge rates in a coin cell with a cathode based on NMC811 (There were 45 cycles in all). HAADF STEM image (c) and distribution maps for germanium (Ge), indium (In) and oxygen (O) for a dendrite formation. 1 – epoxy resin, 2 – dendritic formations.

contact with air. However, due to its rapid degradation under the action of the electron beam, even at low irradiation doses, it was not possible to obtain high-resolution images revealing the atomic structure of the sample.

Finally, Ge NWs powder was used in pouch cell prototyping. Image of the prototype is presented in Figure 6a.

Figure 6b demonstrates charge/discharge curve profiles of the pouch cell at different current and temperature conditions in a voltage range of 2.8–4.2 V. It is seen that at a temperature of +25 °C the pouch cell discharge capacity is of about 330 mAh at discharge current of 70 mA and decreases to 190 mAh at discharge current of 200 mA. The prototype was then tested at a temperature of -20 °C. At a symmetrical charge/discharge current of 200 mA, the discharge capacity is 155 mAh. At the same time, increasing the symmetrical charge/discharge current to 400 mA leads to a decrease in capacity to 75 mAh which is 23% of the nominal capacity at a temperature of +25 °C.

The results approve scalability of described laboratory electrode technology which makes proposed Ge NWs-based electrodes potentially suitable for large-scale production.

anode material at lithiation/delithiation current of 0.125 A/g was approximately 1550 mAh/g. Due to their structure, germanium nanowires can operate at a significantly high current of 32 A/g, providing a specific capacity of 270 mAh/g. It was shown that the coulombic efficiency in all cycling regimes was approximately of 98.5–99 %. This opens up prospects for using the germanium nanowires in lithium-ion batteries with high charge rate.

The cycling data at sub-zero temperature indicate the stability of the electrochemical characteristics of the germanium-based negative electrode. Using 2032 coin cells with a cathode based on NMC811 and an anode based on germanium nanowires, we have demonstrated the ability to charge and cycle the battery at temperatures as low as -40 °C. Thus, the specific capacity of the Ge NWs-based anode was approximately 170 mAh/g at symmetrical current of 0.25 A/g at temperature -40 °C.

The scalability of laboratory-based technology for the production of Ge NWs-based anode material was demonstrated through the example of a pouch cell prototype with a capacity of 330 mAh that was cycled within the temperature range of -20/+25 °C.

## Conclusions

In this work, germanium nanowires were used as an anode material for lithium-ion batteries. The specific capacity of the

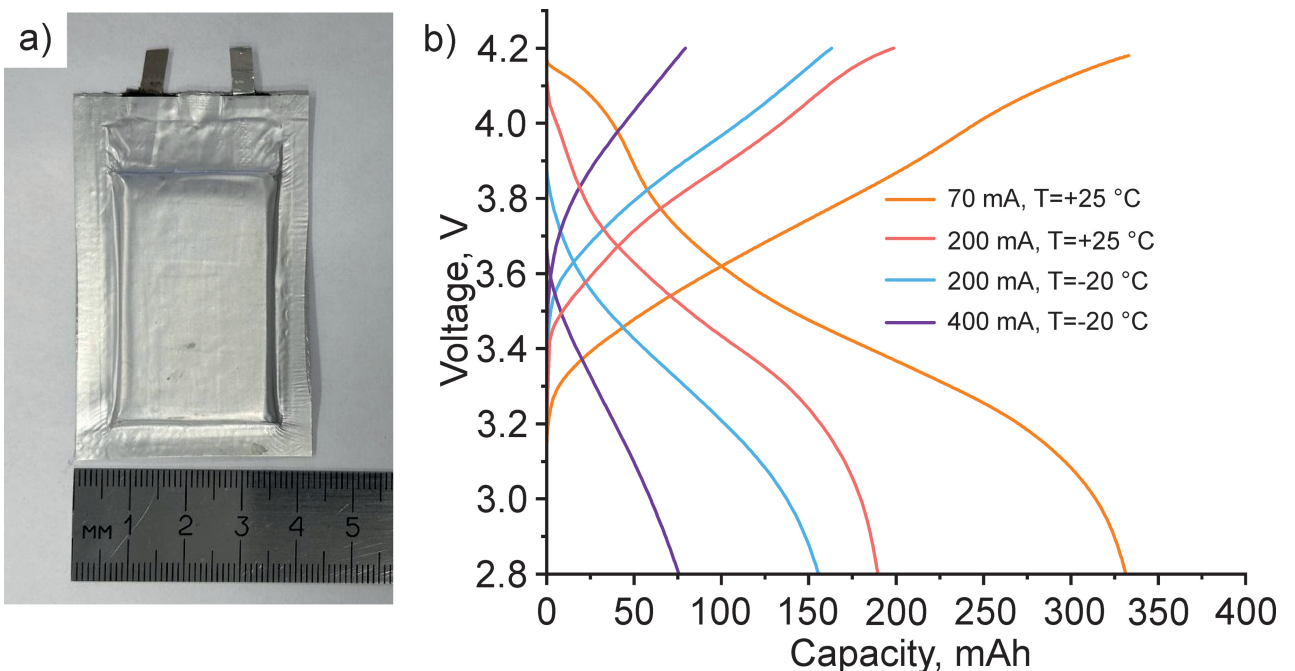


**Figure 6.** Image of the lithium-ion battery prototype with Ge NWs-based anode (a) and charge/discharge curve profiles of the pouch cell at different current and temperature conditions in a voltage range of 2.8–4.2 V (b).

## Material and Methods

### Ge Nanostructures Synthesis

Electrochemical deposition was carried out in a three-electrode cell in two stages. At the first stage, indium seeds were formed from a solution of 0.015 M citric acid and 0.01 M indium chloride ( $\text{InCl}_3$ ). Deposition of the seeds was carried out in galvanostatic mode at  $1 \text{ mA/cm}^2$  for 5 min at  $20^\circ\text{C}$ . In the second stage, germanium was deposited from a solution of 0.1 M  $\text{GeO}_2$ , 0.1 M  $\text{C}_4\text{H}_9\text{O}_4$  and 0.5 M  $(\text{NH}_4)_2\text{SO}_4$ . The deposition was carried out in galvanostatic mode at  $6 \text{ mA/cm}^2$  for 30 min at  $70^\circ\text{C}$ . Copper foil (9  $\mu\text{m}$  thickness, 99.999% purity) was used as a working electrode, which was cut into  $3 \times 3 \text{ cm}$  pieces. A chemically resistant varnish was applied on the back side of the substrate and around the working area. The working area was  $6 \text{ cm}^2$ . A  $3 \times 3 \text{ cm}$  platinum grid was used as the counter electrode and a silver chloride electrode ( $\text{Ag}/\text{AgCl}/3 \text{ M KCl}$ ) was used as the reference electrode. The pH values of the solutions were measured using a HANNA HI 2002-02 pH meter. In all experiments, current density or potential was set using an Autolab PGSTAT302N galvanostat-potentiostat. Currents were normalised to the geometric surface area of the electrode. The temperature of all solutions was controlled using a Termex VT-01 thermostat. Immediately after deposition, the nanostructures were washed with deionised water and dried in argon flow (grade 6.0).

### Samples Physical Characterization

#### Scanning Electron Microscopy (SEM)

The morphology of the obtained samples were studied using scanning electron microscope FEI Helios G4 CX Dual Beam.

### Transmission Electron Microscopy (TEM)

The specimens for transmission electron microscopy (TEM) were prepared also by a Helios NanoLab 650 Dual Beam microscope using the well-known in-situ lift-out focused ion beam (FIB) technique. However, in addition to common electron and ion beam-induced local platinum deposition, Ge nanowires were protected from damage by accelerated ions during the preparation procedure by an M-Bond 610 epoxy glue layer of about 1–2  $\mu\text{m}$  thick applied by a sharp needle as small droplets. The prepared samples were analyzed by TEM using a Titan Themis 200 microscope (FEI, Netherlands) equipped with an image corrector for objective lens spherical aberration (Cs) correction and a Ceta 16 M™ digital camera. TEM studies were performed at an accelerating voltage of 200 kV. A Fischione Model 3000 wide-angle dark field detector was used to obtain images in a high-angle annular dark-field scanning mode (HAADF). The camera length in the STEM mode was about 165 mm. For composition microanalysis, an energy-dispersive X-ray (EDX) detector Super-X was used. The phase composition of the prepared samples was studied using the selected area electron diffraction (SAED) patterns by a Titan Themis 200 microscope (FEI, Netherlands).

### Raman Spectroscopy

Backscattered Raman spectra were measured under excitation with focused laser radiation using a Horiba HR800 micro-Raman spectrometer. In our experiments we used He–Ne laser (wavelength 632.8 nm, maximal power 6 mW, minimal spot radius 3  $\mu\text{m}$ ). The diffraction grating with  $1800 \text{ g mm}^{-1}$  provided spectral resolution of no worse than  $1 \text{ cm}^{-1}$ . The measurement time for one spectrum was 5 s, the number of accumulation was 10 times. The size of Ge nanocrystals was determined by detecting the position of the nanocrystalline Raman peak at a minimum excitation laser intensity to eliminate the heating effect. From the redshift of this peak, we were able to determine the size of nanocrystals in the samples using the corresponding dependence.<sup>[54]</sup>

### Electrochemical Characterization

For the fabrication of cathode, an electrode slurry was used, which included a carbon black, Super C45 as a conductive additive (5% wt.), polyvinylidene difluoride, PVDF (5% wt.) and NMC811 (90% wt.). In order to prepare the electrode slurry, PVDF was dissolved in N-methyl pyrrolidone for 2 hours at 60 °C under stirring. After complete dissolution of the polymer binder, a pre-mixed sample of the active material and the conductive additive was added and stirred on an overhead mixer for 20 hours to form a homogeneous slurry. Next, the obtained electrode slurry was stirred on a vacuum mixer for 20 minutes to remove gaseous substances. After that, the slurry was covered on aluminum foil using Doctor Blade technique and dried at 100 °C for 12 hours until the solvent completely evaporated. After complete drying, the electrode tape was calendered at a temperature of 100 °C with a compression ratio of 20%. Further, electrodes were laser cut on discs with an area of 1.77 cm<sup>2</sup> for 2032 coin cells. Germanium electrodes were used after synthesis without any calendaring.

The positive and negative electrodes were weighed and vacuum dried at a temperature of 120 °C for five hours to remove trace amounts of water and transferred to a glove box, where the coin cells were assembled in an argon atmosphere. Polypropylene membrane Celgard 2500 was used as a separator.

Electrochemical measurements were conducted using Neware battery tester at charge/discharge current density varied in a range of 0.125–2 A/g (1C~1000 mA/g). A mass of germanium film was taken into account. For the half-cell voltage range was of 0.01–3 V. For the full cell with NMC811 cathode voltage range was of 2.8–4.2 V.

1 M solution of LiDFOB in mixture of Propylene carbonate (PC) and Dimethoxyethane (DME) in volumetric ratio 7:3 and addition of 2%wt. of Fluoroethylene carbonate (FEC) and 2%wt. of Vinylene carbonate (VC) was used as an electrolyte.

The measurements of electrolyte ionic conductivity were carried out in electrochemical cell with polished stainless steel blocking electrodes using electrochemical impedance spectroscopy (EIS) method. Frequency range was of 0.5 Hz–1 MHz. Voltage amplitude was of 10 mV. Area of blocking electrode was of 0.79 cm<sup>2</sup>. Distance between electrodes was of 70 µm. The electrolyte ionic conductivity σ was calculated in accordance with the following equation:

$$\sigma = d / (R \times S)$$

where d – distance between blocking electrodes, S – area of the blocking electrode and R – the bulk resistance which is the value corresponding to the intersection point of Nyquist curves with the real axis from EIS data.

### Pouch Cell Fabrication

For the anode slurry preparation, the Ge NWs powder was mixed with conductive additive Super C45 and Carboxymethyl cellulose (CMC) as a binder in deionized water using overhead stirrer during 4 hours. The dry component ratio corresponded to 90% mass. of Ge NWs, 5%mass. of C45 and 5 mass.% of CMC. The negative electrodes were prepared by doctor blade casting of anode slurry onto 9 µm Cu-foil and further dried at 80 °C in air for 24 hours. The areal mass loading of anode with double side coating was of 4 mg/cm<sup>2</sup>. The anode tape was calendered with compression rate of 20% at roll temperature of 100 °C.

The procedure for making the positive electrodes was similar to that described above. In this case, total areal mass loading of

NMC811-based cathode was of 25 mg/cm<sup>2</sup>. For negative and positive electrodes N/P ratio was 1.28.

Calendered electrode tapes were laser cut (wavelength – 1064 nm, power – 10 W, frequency – 20 kHz) into electrodes with size of 2.6×4.3 cm.

Cut anodes and cathodes were then dried in a vacuum oven for 24 hours at 120 °C and about 1 mbar pressure. Then the electrodes were transferred to Ar glove box without contact with ambient for pouch cell assembling. For this purpose, polyethylene separator (Gellek, thickness – 16 µm) has been z-folded between six anodes and seven cathodes using inhouse stacking device. Positive electrodes with single electrode layer were used as the outer electrodes. Current collectors were welded to the electrodes using ultrasonic welding placed in Ar glove box. After the electrode stack has been packed in a case made of 113 µm thick laminated foil, the electrolyte was added using a dispenser at a rate of 2–3 g/Ah. Then the case was evacuated to a pressure of –80 kPa and sealed hermetically. A sealed pouch cell prototype was stored for 24 hours at 25 °C.

After storage, the formation process was carried out in accordance with the following protocol: C/20 CC–CV charge to 4.2 V until C/40 at CV – rest during 10 min – C/20 CC discharge to 2.8 V – rest during 10 min, number of cycles – 3. Here CC and CV abbreviate constant current and constant voltage, respectively.

After the formation process, the pouch cell was repeatedly evacuated to a pressure of –90 kPa and then hermetically sealed.

### Acknowledgements

Part of the work associated with synthesis of Ge material was supported by a grant from Russian Science Foundation No 20-79-10312, <https://rscf.ru/en/project/20-79-10312/>. Part of the work associated with electrochemical measurements and electrolyte synthesis was carried out within the state assignment of Ministry of Science and Higher Education of the Russian Federation (theme No. 1024011500005-1-1.4.5).

### Conflict of Interests

The authors declare no conflict of interest.

### Data Availability Statement

The data that support the findings of this study are available from the corresponding author upon reasonable request.

**Keywords:** lithium-ion batteries • Ge nanowires • lithium insertion • temperature effect • fast lithiation

- [1] H. Luo, Y. Wang, Y.-H. Feng, X.-Y. Fan, X. Han, P.-F. Wang, *Materials* **2022**, *15*, 8166.
- [2] A. Belgibayeva, A. Rakhmetova, M. Rakhatkyzy, M. Kairova, I. Mukushev, N. Issatayev, G. Kalimuldina, A. Nurpeissova, Y.-K. Sun, Z. Bakenov, *J. Power Sources* **2023**, *557*, 232550.
- [3] J. Arai, R. Nakahigashi, *J. Electrochem. Soc.* **2017**, *164*, A3403–A3409.

- [4] G. Zhang, X. Wei, G. Han, H. Dai, J. Zhu, X. Wang, X. Tang, J. Ye, *J. Power Sources* **2021**, *484*, 229312.
- [5] M. Lu, C. Liao, C. Jiang, Y. Du, Z. Zhang, S. Wu, *Electrochim. Acta* **2017**, *250*, 196–202.
- [6] A. Varzi, L. Mattarozzi, S. Cattarin, P. Guerriero, S. Passerini, *Adv. Energy Mater.* **2018**, *8*, 1701706.
- [7] J. Hou, M. Yang, D. Wang, J. Zhang, *Adv. Energy Mater.* **2020**, *10*, 1904152.
- [8] Q. Li, S. Jiao, L. Luo, M. S. Ding, J. Zheng, S. S. Cartmell, C.-M. Wang, K. Xu, J.-G. Zhang, W. Xu, *ACS Appl. Mater. Interfaces* **2017**, *9*, 18826–18835.
- [9] Y. Gao, T. Rojas, K. Wang, S. Liu, D. Wang, T. Chen, H. Wang, A. T. Ngo, D. Wang, *Nat. Energy* **2020**, *5*, 534–542.
- [10] I. D. Johnson, T. E. Ashton, E. Blagovidova, G. J. Smales, M. Lübke, P. J. Baker, S. A. Corr, J. A. Darr, *Sci. Rep.* **2018**, *8*, 4114.
- [11] Q. Li, D. Lu, J. Zheng, S. Jiao, L. Luo, C.-M. Wang, K. Xu, J.-G. Zhang, W. Xu, *ACS Appl. Mater. Interfaces* **2017**, *9*, 42761–42768.
- [12] X. Ding, Y.-X. Li, F. Chen, X.-D. He, A. Yasmin, Q. Hu, Z.-Y. Wen, C.-H. Chen, *J. Mater. Chem. A* **2019**, *7*, 11513–11519.
- [13] J. Xu, X. Wang, N. Yuan, J. Ding, S. Qin, J. M. Razal, X. Wang, S. Ge, Y. Gogotsi, *Energy Storage Mater.* **2019**, *23*, 383–389.
- [14] E. Pohjalainen, T. Rauhala, M. Valkeapää, J. Kallioinen, T. Kallio, *J. Phys. Chem. C* **2015**, *119*, 2277–2283.
- [15] G. Wang, G. Wang, L. Fei, L. Zhao, H. Zhang, *Nano-Micro Lett.* **2024**, *16*, 150.
- [16] Q. Meng, F. Chen, Q. Hao, N. Li, X. Sun, *J. Alloys Compd.* **2021**, *885*, 160842.
- [17] J. Li, Y. Li, Q. Lan, Z. Yang, X.-J. Lv, *J. Power Sources* **2019**, *423*, 166–173.
- [18] Z. Bai, X. Lv, D. Liu, D. Dai, J. Gu, L. Yang, Z. Chen, *ChemElectroChem* **2020**, *7*, 3616–3622.
- [19] X.-H. Ma, X. Cao, Y.-Y. Ye, F. Qiao, M.-F. Qian, Y.-Y. Wei, Y.-D. Wu, Z.-F. Zi, J.-M. Dai, *Solid State Ionics* **2020**, *353*, 115376.
- [20] C. Liang, Y. Tao, N. Yang, D. Huang, S. Li, K. Han, Y. Luo, H. Chen, L. Mai, *Electrochim. Acta* **2019**, *311*, 192–200.
- [21] L. Yu, S.-X. Zhao, Y. Yuan, G.-D. Wei, *Electrochim. Acta* **2021**, *384*, 138351.
- [22] Z. Syum, T. Billo, A. Sabbah, B. Venugopal, S.-Y. Yu, F.-Y. Fu, H.-L. Wu, L.-C. Chen, K.-H. Chen, *ACS Sustainable Chem. Eng.* **2021**, *9*, 8970–8979.
- [23] K. Richter, T. Waldmann, N. Paul, N. Jobst, R. Scurtu, M. Hofmann, R. Gilles, M. Wohlfahrt-Mehrens, *ChemSusChem* **2020**, *13*, 529–538.
- [24] T. Subburaj, W. Brevet, F. Farmakis, D. Tsiplakides, S. Balomenou, N. Stratakis, C. Elmasides, B. Samaniego, M. Nestoridi, *Electrochim. Acta* **2020**, *354*, 136652.
- [25] J. Chen, Y. Liu, F. Meng, S. He, J. Liu, Y. Zhao, K. Song, R. Hu, M. Zhu, *Nano Energy* **2024**, *129*, 110048.
- [26] K. Yan, J. Wang, S. Zhao, D. Zhou, B. Sun, Y. Cui, G. Wang, *Angew. Chem.* **2019**, *131*, 11486–11490.
- [27] A. J. Morris, C. P. Grey, C. J. Pickard, *Phys. Rev. B* **2014**, *90*, 054111.
- [28] J. Sangster, A. D. Pelton, *JPE* **1997**, *18*, 289–294.
- [29] W. Lang, C. Yue, M. Dang, G. Wang, Y. Chen, F. Hu, Z. Liu, J. Shu, *J. Power Sources* **2023**, *560*, 232706.
- [30] S. K. Marka, S. Petnikota, M. V. Reddy, S. Adams, V. V. Satya Siva Srikanth, *J. Alloys Compd.* **2023**, *960*, 170766.
- [31] A. Verdianto, H. Jung, S.-O. Kim, *Materials Today Advances* **2024**, *21*, 100472.
- [32] X.-M. Pham, S. Abdul Ahad, N. N. Patil, H. Geaney, S. Singh, K. M. Ryan, *Nanoscale Horiz.* **2024**, *9*, 637–645.
- [33] C. Jo, B. Wen, H. Jeong, S. K. Park, Y. Son, M. De Volder, *ACS Nano* **2023**, *17*, 8403–8410.
- [34] T. Omae, T. Yamada, D. Fujikake, T. Kozawa, G. Uchida, *Appl. Phys. Express* **2024**, *17*, 026001.
- [35] E. Conwell, *Proc. IRE* **1958**, *46*, 1281–1300.
- [36] J. Graetz, C. C. Ahn, R. Yazami, B. Fultz, *J. Electrochem. Soc.* **2004**, *151*, A698.
- [37] C.-Y. Chou, G. S. Hwang, *J. Power Sources* **2014**, *263*, 252–258.
- [38] X. Xiao, X. Li, S. Zheng, J. Shao, H. Xue, H. Pang, *Adv. Mater. Interfaces* **2017**, *4*, 1600798.
- [39] L. C. Loaiza, L. Monconduit, V. Seznec, *Small* **2020**, *16*, 1905260.
- [40] X. Liu, X.-Y. Wu, B. Chang, K.-X. Wang, *Energy Storage Mater.* **2020**, *30*, 146–169.
- [41] X. X. Fang, C. Jiang, C. Yue, F. Hu, *Chem. Eur. J.* **2024**, *30*, e202400063.
- [42] G. A. Collins, K. McNamara, S. Kilian, H. Geaney, K. M. Ryan, *ACS Appl. Energ. Mater.* **2021**, *4*, 1793–1804.
- [43] S. Choi, Y. Cho, J. Kim, N. Choi, H. Song, G. Wang, S. Park, *Small* **2017**, *13*, 1603045.
- [44] I. M. Gavrilin, Yu.O. Kudryashova, A. A. Kuz'mina, T. L. Kulova, A. M. Skundin, V. V. Emets, R. L. Volkov, A. A. Dronov, N. I. Borgardt, S. A. Gavrilov, *J. Electroanal. Chem.* **2021**, *888*, 115209.
- [45] T. L. Kulova, I. M. Gavrilin, Y. O. Kudryashova, A. M. Skundin, *Mendeleev Commun.* **2020**, *30*, 775–776.
- [46] S. Jurng, Z. L. Brown, J. Kim, B. L. Lucht, *Energy Environ. Sci.* **2018**, *11*, 2600–2608.
- [47] Q. Dong, F. Guo, Z. Cheng, Y. Mao, R. Huang, F. Li, H. Dong, Q. Zhang, W. Li, H. Chen, Z. Luo, Y. Shen, X. Wu, L. Chen, *ACS Appl. Energ. Mater.* **2020**, *3*, 695–704.
- [48] Y. Zhu, Y. Li, M. Bettge, D. P. Abraham, *J. Electrochem. Soc.* **2012**, *159*, A2109–A2117.
- [49] X. Zhang, X. Cheng, X. Chen, C. Yan, Q. Zhang, *Adv. Funct. Mater.* **2017**, *27*, 1605989.
- [50] E. Markevich, G. Salitra, F. Chesneau, M. Schmidt, D. Aurbach, *ACS Energy Lett.* **2017**, *2*, 1321–1326.
- [51] J. Lee, Y.-J. Kim, H. S. Jin, H. Noh, H. Kwack, H. Chu, F. Ye, H. Lee, H.-T. Kim, *ACS Omega* **2019**, *4*, 3220–3227.
- [52] S. Dalavi, P. Guduru, B. L. Lucht, *J. Electrochem. Soc.* **2012**, *159*, A642–A646.
- [53] T. L. Kulova, I. M. Gavrilin, Y. O. Kudryashova, A. M. Skundin, S. A. Gavrilov, *Mendeleev Commun.* **2021**, *31*, 842–843.
- [54] D. L. Goroshko, I. M. Gavrilin, S. V. Chusovitina, A. A. Dronov, R. L. Volkov, A. V. Gerasimenko, N. I. Borgardt, S. A. Gavrilov, *Appl. Surf. Sci.* **2024**, *655*, 159677.
- [55] E. B. Gorokhov, *Semiconductors* **2005**, *39*, 1168.

Manuscript received: November 26, 2024

Revised manuscript received: February 28, 2025

Accepted manuscript online: March 2, 2025

Version of record online: March 21, 2025